Supplementary Materials

Experimental Set-up

Control of the Exoskeleton System

All the experiments carried out in the study were performed using the exoskeleton system for robot-assisted gait rehabilitation shown in Figure S01 (37) (Lokomat by Hocoma AG, Zurich, Switzerland). The system allows one to control the subject's hip and knee flexion/extension movements during walking on a treadmill. A control modality referred to as path control (38) was used during the experiments. The path control technique relies upon an algorithm that continuously compares the subject's gait pattern to a reference gait pattern and either actively drives the system to minimize the interaction forces between the subject and the robot or generates a force to affect the subject's lower-limb movements.

The generalized elasticity method proposed by Vallery et al (35) was used to minimize the effects of the inertia of the exoskeleton system on the gait patterns of individuals walking with their lower limbs strapped to the robotic legs of the exoskeleton. This approach utilizes the subject's own gait pattern and a model of the exoskeleton to generate a set of radial-basis functions. The radial-basis functions act as virtual springs that minimize the subject's effort required to move the exoskeleton along the gait trajectory.

The characteristics of the gait patterns of each individual were recorded during the first trial of each experimental session for the purpose of estimating the optimal positions and spring coefficients of the virtual springs utilized according to the method proposed by Vallery et al (35). Subjects were instructed to walk with their lower limbs strapped to the exoskeleton at a speed of 3 km/h for approximately 60 s while paced by a metronome as explained below. The average trajectory of motion of the lower limbs during this trial was used for the above-mentioned calculations.

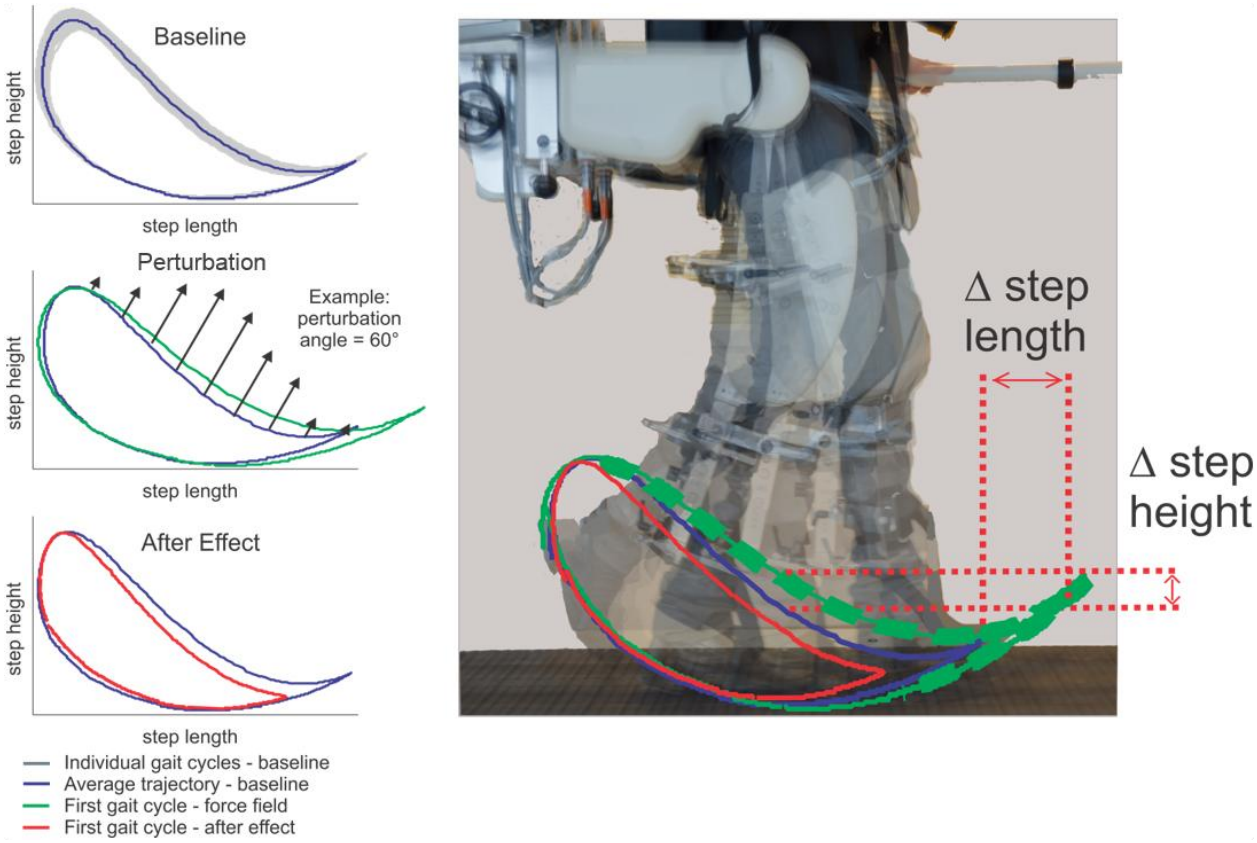

Figure S01: Schematic representation of the motor adaptation experiments. *The plots on the left show the foot trajectory in a Cartesian coordinate system whose origin was located in correspondence of the center of rotation of the exoskeleton hip joint. The plot showing the foot trajectory for the perturbation phase of the experiment also shows a schematic representation of an example of the velocity-dependent perturbation force vector. The plot on the right shows the foot trajectory for the three phases of the experiments. The trajectory in blue represents the baseline data, the one in green corresponds to the perturbation data, and the one in red represents the aftereffect foot trajectory. The thick dashed green line represents the portion of the gait cycle during which the robot generates a perturbation. The plot also shows how the changes in step length and step height were estimated. See text for details.*

The reference gait pattern of motion for the path control algorithm (38) was then determined on a subject-by-subject basis during the second trial of each experimental session using the settings derived from the first trial. This approach allowed us to derive the reference gait pattern of motion for the path control algorithm (38) when the interaction forces between the subject and the robot were minimum. During the second trial, subjects were instructed to walk at a speed of 3 Km/h for approximately 120 s while paced by a metronome.

To determine at any given point in time where in the gait cycle the subject was at, we used an algorithm previously proposed by Aoyagi et al (39). This technique is based on estimating the vector norm between the current position and velocity in the hip vs. knee joint space and the position and velocity values of the reference gait pattern of motion. By identifying the minimum of this vector norm, the algorithm allows one to robustly detect the position on the reference trajectory that corresponds to the current position of the gait cycle the subject is at.

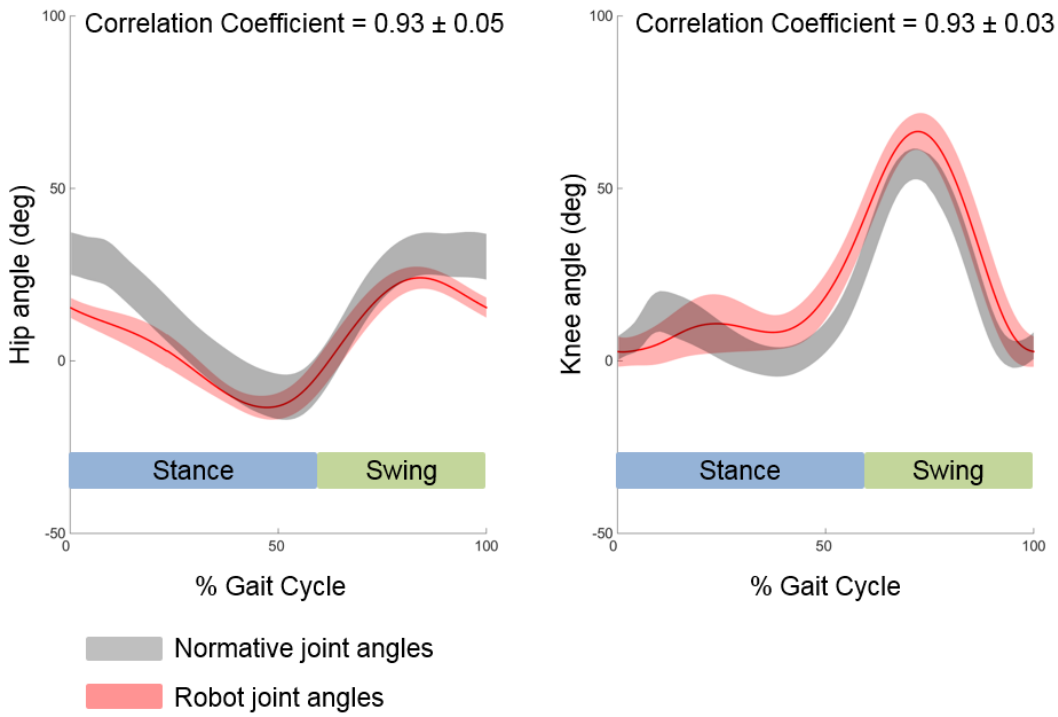

Figure S02: Comparison of the robot joint angles during the baseline phase of the experiments and normative joint angle data collected during over-ground walking. *Hip (left plot) and knee (right plot) flexion/extension patterns observed during the baseline phase of the experiments (red) and hip and knee flexion/extension patterns observed during over-ground walking (gray). The data is shown as average ± standard deviation. The over-ground walking data was collected from 88 healthy individuals using a camera-based motion capture system (VICON, Oxford UK). The plots show a high degree of similarity between the data collected during the baseline phase of the experiments and the data collected during over-ground walking.*

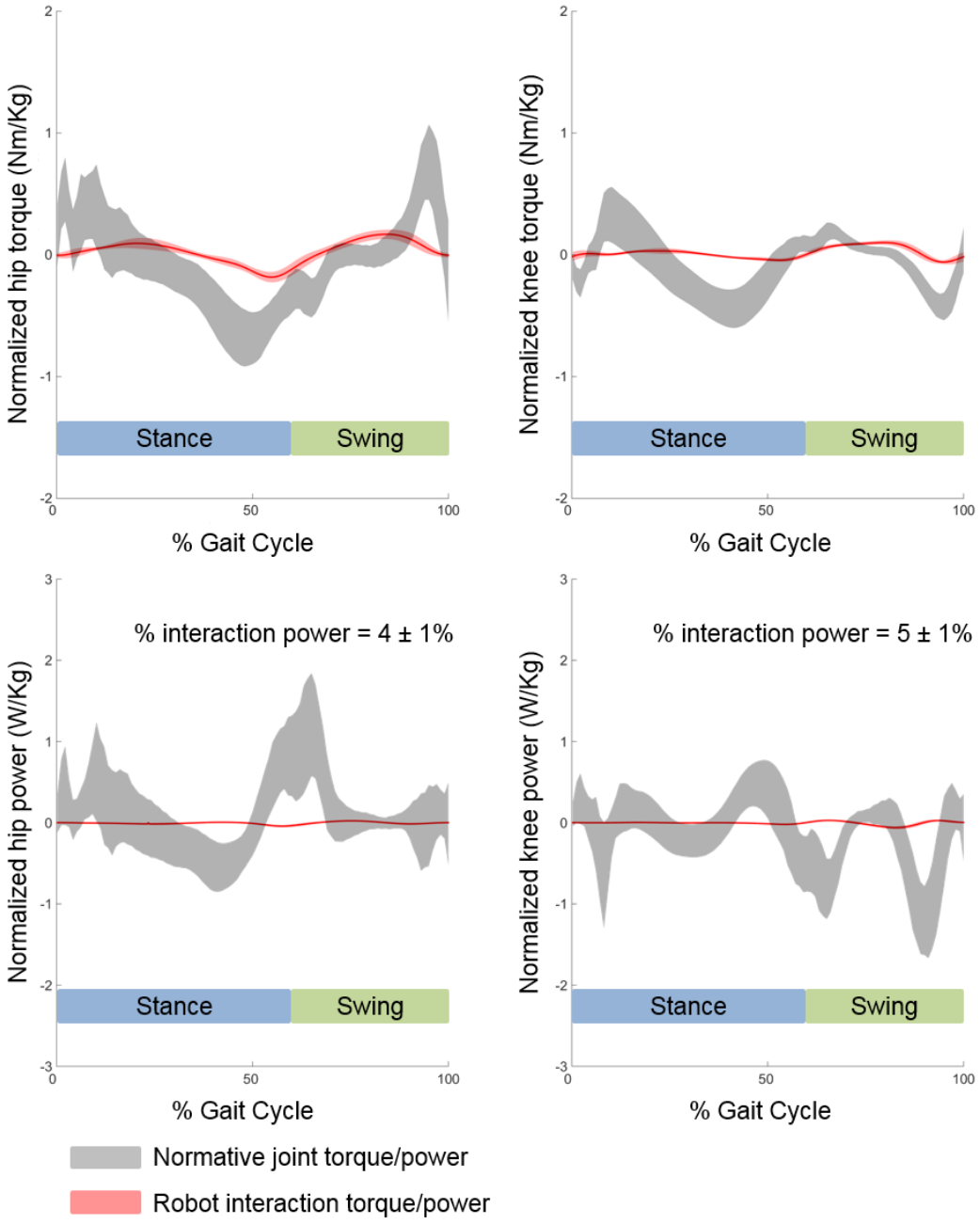

Figure S03: Comparison of joint interaction torque and power values during the baseline phase of the experiments and normative data collected during over-ground walking. *Top plots: hip (left plot) and knee (right plot) interaction torques during the baseline phase of the experiments (red) and during over-ground walking (gray). The interaction torque values are small compared to the values observed during over-ground walking. Bottom plots: hip (left plot) and knee (right plot) interaction power values during the baseline phase of the experiments (red) and during over-ground walking (gray). The interaction power values are small compared to the values observed during over-ground walking. The data is shown as average ± standard deviation. The normative data was collected from 88 healthy individuals using a motion capture system (VICON, Oxford UK).*

Interaction between the Subjects and the Robot

We evaluated the effectiveness of the above-described control approach by comparing gait patterns observed during the baseline phase of the experiments and gait patterns observed in a group of 88 healthy subjects during over-ground walking. The normative data during over-ground walking was collected using a camera-based motion capture system (VICON, Oxford UK).

Figure S02 shows a comparison between the hip and knee joint angles recorded during the baseline phase of the experiments (when subjects walked on a treadmill with their legs strapped to the robotic system) and the normative data collected during over-ground walking.

Small deviations from the normative data are shown at the hip at the initial contact and terminal swing phases of the gait cycle. Small deviations from the normative data are also shown at the knee during the terminal stance and mid-swing phases of the gait cycle. These observations are likely due to the mechanical constraints of the robotic system, i.e. the fact that the system does not allow the rotation of the pelvis around any of the three axes (i.e. tilt, obliquity and rotation) and the fact that the movement at the hip and knee is constraint to the sagittal plane. Nonetheless, the patterns of movement at the hip and knee observed during the baseline phase of the experiments appear to show only minor deviations from the patterns of movement observed during over-ground walking.

To quantify the similarity among these patterns, we estimated the Pearson correlation coefficient between the average hip/knee flexion/extension patterns derived for each subject at baseline and the average normative angular displacements observed during over-ground walking. The Pearson correlation coefficients were 0.93 ± 0.05% for the hip and 0.93 ± 0.03% for the knee.

To assess if the above-described control approach also led to negligible interaction forces between the subjects and the robot, we estimated the interaction torque and power trajectories at the hip and knee during the baseline phase of the experiments. We then compared the magnitude of such interaction torque and power trajectories with the torque and power trajectories derived during over-ground walking from the above-mentioned dataset recorded during over-ground walking. Figure S03 shows the comparison among these torque and power trajectories. These comparisons allow us to conclude that the torque and power trajectories measured by monitoring

the interaction between the subjects and the robot are of negligible magnitude compared to the magnitude of the torque and power trajectories associated with over-ground walking. Specifically, the integral of the absolute values of the joint interaction power trajectories account for just 4 ± 1% and 5 ± 1% of the power generated during gait at the hip and knee respectively.

Generation of Mechanical Perturbations

The above-described control schema was applied to the left robotic leg during all the experiments. The same control modality was applied to the right robotic leg for all the steps but for those ones during which a mechanical perturbation was produced by the robot, namely randomly selected steps during the single-step perturbation experiments and all the steps during the perturbation phase of the motor adaptation experiments. Mechanical perturbations were produced by generating appropriate torques using the actuators at the hip and knee joints of the robotic leg. Torque values were chosen to lead to a given net effect at the distal end of the right robotic leg hence affecting the foot trajectory of motion. The torques generated by the robotic legs led to a resultant force vector that we named the perturbation force vector. The magnitude and orientation of the desired perturbation force vector in a Cartesian coordinate system located at the hip joint of the robotic leg were computed using the following formula

$$(t) = \begin{bmatrix} {}_{x}(t) \\ F_y(t) \end{bmatrix} = \begin{bmatrix} A & 0 \\ B & 0 \end{bmatrix} \begin{bmatrix} v_x(t) \\ v_y(t) \end{bmatrix} \qquad \text{Equation S01}$$

In this equation, F(t) is the perturbation force vector, F_x and F_y are the x (i.e. antero-posterior direction) and y (i.e. vertical direction) components of the perturbation force vector, A and B are the viscous damping coefficients, and v_x and v_y are the x and y components of the velocity of the distal end of the robotic leg. Since the exoskeleton utilized in this study has sensors only at the hip and knee joints of the robotic legs, the Jacobian was used to estimate the instantaneous velocity vector in the above-mentioned Cartesian coordinate system from the angular displacement measures gathered using the sensors of the robotic leg. The position of the distal end of the robotic leg was estimated from the angular displacement values gathered from the sensors of the robotic leg using the following inverse kinematics Jacobian

$$\begin{bmatrix} x \\ y \end{bmatrix} = \begin{bmatrix} lthigh \\ lshank \end{bmatrix} * \begin{bmatrix} sin\theta_h & \sin\ \theta_h - \theta_{k)} \\ cos\theta_h & \cos\ \theta_h - \theta_{k)} \end{bmatrix}$$ Equation S02

where x and y represent the position of the distal end of the robotic leg in the Cartesian coordinate system located at the hip joint of the robotic leg. Also, θ_h and θ_k are the angular displacements at the hip and knee, respectively. l_{thigh} and l_{shank} represent the length of the thigh and shank segments of the robotic leg. Velocity estimates v_x and v_y were computed by estimating the first derivative of the x and y position estimates.

In all the experiments, the viscous damping coefficients A and B in Eq. S01 were computed as $\mathrm{A} = 0.115 \cdot \cos(\propto) \cdot \mathrm{Sm}$, $\mathrm{B} = 0.690 \cdot \sin(\propto) \cdot \mathrm{Sm}$, where $\propto$ is the orientation of the perturbation force vector and Sm is the subject's mass in kg. The constant values (i.e. 0.155 and 0.690) used to calculate the damping coefficients A and B were empirically identified during a series of exploratory experiments aimed to assess the magnitude of robot-generated forces able to induce substantial deviations in the right foot trajectory from its baseline trajectory without causing subjects to stumble (8).

A time window was applied to the torques to be generated by the actuators at the hip and knee joints of the right robotic leg so that the perturbations were generated only during a portion of the gait cycle that corresponded approximately to the swing phase. The portion of the trajectory of movement of the foot affected by the robot-induced perturbation is highlighted in Figure S01 (thick dashed green line in the right panel). The time window applied to the torques to be generated by the actuators at the hip and knee joints of the right robotic leg had a time support starting at the point of the gait cycle when the estimated foot velocity in the antero-posterior direction turned from negative to positive ($V_x(t) > 0|_{Vx(t-1) < 0}$) and ending at the point when the position of the foot in the antero-posterior direction turned from positive to negative ($x(t) < 0|_{x(t-1)>0}$). The first of these points corresponded approximately to the beginning of the swing phase, i.e. the foot-off time. The second of these points corresponded approximately to the heel-strike instance. In addition, we applied a rate limiter of -10 Nm/s and 7 Nm/s to the magnitude of the torques generated by the hip and knee actuators, respectively. The rate limiter allowed us to ensure a smooth transition when switching the perturbation force vector on and off. The values used by this module to limit the rate of change of the torques generated by the hip and knee actuators were determined during prior exploratory

studies (8). In such studies, we aimed to achieving a smooth transition between the portion of the gait cycle during which a perturbation was generated by the robot and the portion of the gait cycle when the system was controlled to minimize the interaction forces between the subjects and the robot.

All the software modules were implemented using Matlab 2011b (The Mathworks, Natick, USA, www.mathworks.com). Figure S04 shows a block diagram of the control schema that we used to drive the robotic exoskeleton utilized in the study.

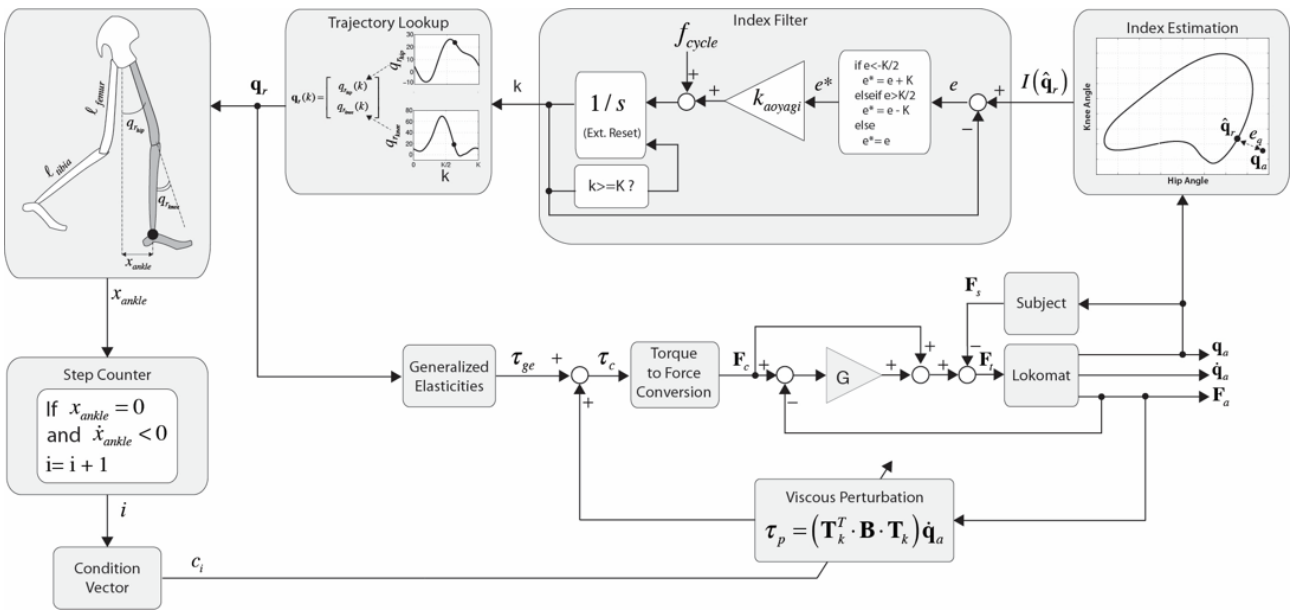

Figure S04: Diagram of the controller of the exoskeleton. *Left and right legs were controlled independently. The controller supported three modes of operation: baseline, perturbation, and aftereffect. A condition vector determined when the perturbation force vector was applied. During the baseline and aftereffect phases, an index estimation algorithm determined the current position of the lower limbs in the gait cycle thus enabling the calculation of the generalized elasticity coefficients using a trajectory lookup table.*

Pacing Subjects with a Metronome

Because the mechanical perturbations utilized during the study were generated using a velocity-dependent perturbation force vector, we had to ensure that the velocity of movement during the swing phase of the gait cycle showed as little variability as possible. We accomplished this goal by minimizing the variability of the subjects' ankle velocity using an electronic metronome

to pace their cadence. Specifically, we asked subjects to pace their heel-strikes according to the beats of the metronome, which we set to a period of 0.7 s (85.7 bpm). We had determined in preliminary exploratory experiments that such metronome frequency led to a comfortable walking speed (8). Subjects had to keep the timing of the swing phase consistent across gait cycles in order to keep up with the metronome pace. As a result, all subjects experienced comparable magnitudes of the perturbation force vectors during the experiments. To evaluate the effectiveness of the proposed approach, we tested the effect of the metronome on the ankle velocity in the antero-posterior direction. It is worth emphasizing that the ankle velocity in the antero-posterior direction was used to calculate the magnitude of the perturbation. These data collections took place in five of the subjects who later participated in the single-step perturbation experiments. Specifically, we collected data during two trials consisting of 50 gait cycles each. During these trials, the robotic system was controlled as done during the baseline phase of the experiments. This approach allowed us to achieve a significant reduction in the variability of the ankle velocity in the antero posterior direction for all five subjects but one (Figure S05). We observed an average

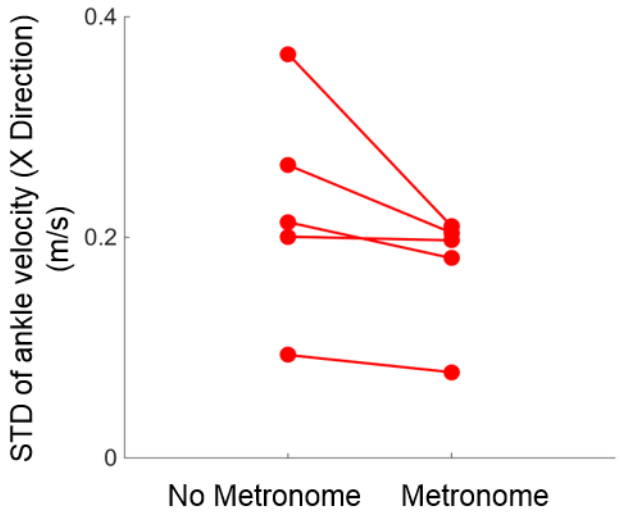

Figure S05: Effect of the metronome on the variability in the ankle velocity. *The plot shows the variability in ankle velocity in the antero-posterior direction recorded from 5 subjects during baseline walking with and without pacing with a metronome set at 85.7 bpm. The variability in the ankle velocity was calculated as the standard deviation (STD) of the ankle velocity during swing. All five subjects but one showed a significant decrease in ankle velocity variability due to the presence of the metronome as acoustic cue.*

reduction in the variability of the ankle velocity in the antero posterior direction of 6 cm/s.

Experimental Procedures

All the experimental sessions began with two trials. These two trials aimed to choosing optimal settings for the generalized elasticity method proposed by Vallery et al (35) and to determining the reference gait pattern of motion for the path control algorithm (38) that we used during the experiments. These trials were followed by single-step perturbation trials or motor adaptation trials as described in the following.

Single-Step Perturbation Experiments

We studied the effects of single-step perturbations in 9 male and 6 female subjects with age 32.7 ± 8.0 years (mean ± standard deviation), weight 74 ± 14 kg, and height 174 ± 11 cm. These experiments allowed us to determine the relationship between the orientation of the perturbation force vector in the sagittal plane and the resulting changes in step length and height. The perturbation space of 360° in the sagittal plane was sampled at intervals of 20° resulting in 19 testing conditions. Tests performed with a perturbation force vector with orientation equal to 0° corresponded to a forward perturbation (i.e. positive x-axis direction). Tests performed with a perturbation force vector with orientation equal to 360° were equivalent to those performed at 0°. Tests performed with a perturbation force vector with orientation equal to 90° corresponded to an upward perturbation (i.e. positive y-axis direction). Subjects were instructed to walk at 3 km/h with their lower limbs strapped to the exoskeleton legs. The robotic legs were controlled to minimize the interaction between the subjects and the robot for all the gait cycles but those ones randomly selected to generate a single-step perturbation of the right foot trajectory. The orientation of the perturbation force vector was randomly selected among one of the above-mentioned 19 orientation values of the perturbation force vector. The steps during which the robot generated a perturbation were selected randomly, allowing n gait cycles ($[5<n<8]$) in between perturbations. The trial during which 19 steps were selected to generate perturbations with different values of the orientation of

the perturbation force vector was repeated four times per subject to obtain a sample of four right steps for each value of the 19 selected orientation values of the perturbation force vector. These trials consisted of 770 gait cycles. Step-length and step-height values of the four data points collected for each value of the orientation of the perturbation force vector were normalized by the step-length and step-height values recorded at baseline for each subject and averaged to generate a single data point per subject. These values were then averaged across subjects and interpolated using cubic spline functions to estimate the effects on step length and step height of all the possible values of the orientation of the perturbation force vector. These estimated curves were used to determine the approximate orientation values for the six conditions tested in the motor adaptation experiments. The six values of the orientation of the perturbation force vector to be tested during the motor adaptation experiments were selected to lead to the following effects: an increase in step length with no effect on step height (X testing condition); a decrease in step length with no effect on step height (X_{inv} testing condition); an increase in step height with no effect on step length (Y testing condition); a decrease in step height with no effect on step length (Y_{inv} testing condition); a combined effect on step length and step height with maximum deviation from baseline step length (X_{max} testing condition); and a combined effect on step length and step height with maximum deviation from baseline step height (Y_{max} testing condition).

Motor Adaptation Experiments

We studied the effects of perturbations generated by the exoskeleton over multiple steps in 10 male and 5 female subjects, age 30.5 ± 6.5 years (mean ± standard deviation), weight 72 ± 10 kg, and height 174 ± 9 cm. Thirteen subjects participated in the single-step perturbation experiments and in the motor adaptation experiments. The motor adaptation experiments took place in two sessions. During each of these sessions we tested the effects of three different values of the orientation of the perturbation force vector in three separate trials. Each motor adaptation trial consisted of 420 gait cycles. Subjects were first instructed to walk for 20 gait cycles to get used to walking on the treadmill with their lower limbs strapped to the robotic legs of the exoskeleton. During these first 20 gait cycles, the exoskeleton was controlled using the above-described control

schema to minimize the interaction between the subjects and the robot. During the following 160 gait cycles, the robot was controlled using the same control schema for all the steps but nine randomly selected steps during which the robot generated a perturbation. Specifically, the robot generated 9 single-step perturbations interspersed every n steps, with $8<n<17$. All perturbations were generated with the same orientation of the perturbation force vector. The step-length and step-height values observed during these 9 single-step perturbations were later used to estimate the effect of the perturbations before an adaptation could occur. These values were later averaged with the step-length and step-height values for the first step of the perturbation phase of the experiments. This approach led to an improvement in the quality of the estimates of the parameters of the exponential fitting for the perturbation phase of the experiments. During the following 80 gait cycles, the exoskeleton was again controlled using the control schema utilized to minimize the interaction between the subjects and the robot. We refer to this phase of the experiment as the baseline phase. Then subjects were exposed to the velocity-dependent perturbation force vector for 80 consecutive gait cycles. We refer to this phase of the experiment as the perturbation phase. Each trial used a different orientation of the perturbation force vector randomly selected among the above-listed six values. For each trial, the orientation of the perturbation force vector used during the perturbation phase of the experiment was the same as the orientation of the perturbation force vector used during the 9 single-step perturbations performed before the baseline phase of the experiment. Finally, subjects were instructed to walk for additional 80 gait cycles during which the exoskeleton was controlled using the same algorithm used during the baseline phase of the experiment. We refer to this phase of the experiment as the aftereffect phase. Figure S01 shows a graphical representation of the effects on the trajectory of the right foot for the baseline, perturbation and aftereffect phases of the motor adaptation experiments.

Data Analysis

Step Length and Height Changes in Response to Robot-Induced Perturbations

The effect of the perturbation force vector $F(t)$ on the subjects' gait patterns of movement was quantified by estimating the magnitude of the changes in step length and step height observed during the perturbation and aftereffect phases of the experiments compared to the baseline data. Kinematic and kinetic data was sampled at 1 kHz and recorded in the internal memory of the exoskeleton system and downloaded at completion of the experiments. Measures of deviation from baseline in step length ΔL were computed according to the following formula

$$\Delta L = \max(x_{Cond}) - \max(x_{Baseline});\ Cond\ \epsilon\ [Perturbation, AfterEffect] \qquad \text{Equation S03}$$

All measures of deviation from baseline in step height ΔH were computed according to the following formula

$$\Delta \mathrm{H} = y_{Cond}\ x = 0) - y_{Baseline}\ x = 0);\ Cond\ \epsilon\ [Perturbation, AfterEffect]. \qquad \text{Equation S04}$$

where x=0 corresponded to mid-swing when the foot was vertically aligned with the center of rotation of the hip joint of the exoskeleton.

The single-step perturbation experiments allowed us to estimate the average displacement in step length and step height associated with different values of the orientation of the perturbation force vector. The motor adaptation experiments allowed us to observe the motor behaviors associated with exposure to a perturbation force vector over multiple consecutive steps and the residual effects after removal of the perturbation force vector. In the upper extremities, perturbation and aftereffect related kinematic changes were shown to typically follow exponential trajectories (40). Since we observed similar behaviors in our lower-limb adaptation experiments, we computed step-length and step-height deviation from baseline on a step-by-step basis and fitted an exponential curve to the data collected during the perturbation and aftereffect phases according to the following formulas

$$c_{Perturbation}\ n) = a(1 - \exp\left(\frac{n}{\tau}\right)) + \varepsilon(n). \qquad \text{Equation S05}$$

$$c_{AfterEffect}\ n) = b\exp\left(-\frac{n}{\tau}\right) + d + \varepsilon(n)$$ Equation S06

where *c* is the adaptation coefficient at step n, *a* and *b* are scalar values, τ is the adaptation time constant, *d* the y-axis intercept, and ε the value at the end of each phase of the experiments. For the perturbation phase for each trial, the parameter *a* was estimated as the average of the nine single-step perturbations performed at the beginning of the trial and the first step of the perturbation phase of the experiment. τ was estimated using a least-squares algorithm. For the aftereffect phase, all three parameters were estimated using the least-squares method. Exponentials were fitted on both averaged aggregate data and the data of each single subject.

We evaluated the percentage amount of adaptation in step length (SL) and step height (SH) as:

$$Adaptation_{SL/SH} = \frac{M(1^{st}step\ of\ Perturbation) - M(last\ step\ of\ Perturbation)}{M(1^{st}step\ of\ Perturbation) - \overline{M(baseline)}} \cdot 100$$ Equation S07

where *M* is the desired metric (i.e. step length – SL - or step height - SH).

Analysis of the Mechanical Work Performed by the Subjects

As an indirect measure of energy consumption, we estimated the net mechanical work performed by the subjects at different points of the experiment. The net mechanical work was estimated from the angular displacements and the interaction torques recorded by the exoskeleton at each joint. The net work at baseline $Work_{\boldsymbol{BL}}$ was estimated for each step of the last 10 steps of the baseline phase as:

$$Work_{\boldsymbol{BL}} = \sum_{i=1}^{N} \tau_{hipBL}\ i) \cdot \Delta\theta_{hipBL}\ i) + \sum_{i=1}^{N} \tau_{kneeBL}\ i) \cdot \Delta\theta_{kneeBL}\ i)$$ Equation S08

where τ_{hipBL} and τ_{kneeBL} are the torques at the hip and knee, $\Delta\theta_{hipBL}$ and $\Delta\theta_{kneeBL}$ are the angular displacements at the hip and knee, and *N* is the number of samples for one step. The data was re-sampled so that we had 500 samples for each step. The work performed by the subject to counter the robot-induced perturbations $Work_{Pertsubj}$ (Eq. S08) was estimated as the difference between the work calculated from the torques and angles measured by the exoskeleton during the final ten steps of the perturbation phase $Work_{\boldsymbol{Perttot}}$ and the estimated work related only to the robot-

induced perturbation $Work_{\boldsymbol{robotpert}}$. The former - $Work_{\boldsymbol{Perttot}}$ - was derived similarly to $Work_{\boldsymbol{BL}}$ using the torque values at the hip $\tau_{hipPert}$ and knee $\tau_{kneePert}$ ad well as the angular displacements at the hip $\Delta\theta_{hipPert}$ and knee $\Delta\theta_{kneePert}$ measured by the exoskeleton (Eq S10). The latter - $Work_{\boldsymbol{robotpert}}$ - was estimated from the perturbation torques at the hip $\tau_{hiprobotpert}$ and knee $\tau_{kneerobotpert}$ and the angular deviations caused by the perturbation. Such angular deviations at the hip θ_{hipSS} and knee θ_{kneeSS} were estimated first by computing the average angles during the nine single-step perturbations and the first step of the perturbation phase (when no adaptation had taken place as yet). Then we derived the difference between these estimates and the average hip θ_{hipBL} and knee θ_{kneeBL} angles at baseline. The following formulas show how we derived $Work_{Pertsubj}$, $Work_{\boldsymbol{Perttot}}$, and $Work_{\boldsymbol{robotpert}}$.

$$Work_{Pertsubj} = Work_{\boldsymbol{Perttot}} - Work_{\boldsymbol{robotpert}} \quad \text{Equation S09}$$

$$Work_{\boldsymbol{Perttot}} = \sum_{i=1}^{N} \tau_{hipPert}\ i) \cdot \Delta\theta_{hipPert}\ i) + \sum_{i=1}^{N} \tau_{kneePert}\ i) \cdot \Delta\theta_{kneePert}\ i) \quad \text{Equation S10}$$

$$Work_{\boldsymbol{robotpert}} = \sum_{i=1}^{N} \tau_{hiprobotpert}\ i) \cdot \Delta(\theta_{hipSS}\ i) - \theta_{hipBL}\ i)) + \sum_{i=1}^{N} \tau_{kneerobotpert}\ i) \cdot \Delta(\theta_{kneeSS}\ i) - \theta_{kneeBL}\ i)) \quad \text{Equation S11}$$

Statistical analyses were performed to detect significant changes in net mechanical work for each condition using the Wilcoxon's signed rank test.

Symmetry Indices

We calculated symmetry indices to assess if the observed motor behaviors were marked by symmetry in the gait kinematics and/or kinetics. The following are the parameters for which we derived the symmetry indices.

1) Non-normalized step length, calculated as:

$$SL = \max(x) \quad \text{Equation S12}$$

2) Non-normalized step height, calculated as:

$$SH = y(x = 0); \quad \text{Equation S13}$$

3) Net mechanical work calculated according to the Eq. S08-S11.

These parameters were calculated for the last ten steps of the baseline phase and the last ten steps of the perturbation phase for both the right and left lower limbs.

Symmetry indices *SI* were derived for all the above-listed parameters as:

$$SI = {P_{right}}/{P_{left}} \qquad \text{Equation S14}$$

where $P_{right,left}$ is one of the above-listed parameters for the right and left lower limbs, respectively. Wilcoxon's signed rank tests were performed to detect significant differences in the symmetry indices between the end of the baseline phase and the end of the perturbation phase of the experiments.

Statistical Analyses

We performed statistical comparisons of the changes in step length and step height observed during the adaptation experiments for both the right leg (the one the robot applied a perturbation force vector to) and the left leg (the one that was not subject to a perturbation). Statistical analyses were performed using Friedman non parametric tests followed by post-hoc analyses based on the Minimum Significant Difference (MSD) test to assess statistically significant pair-wise differences when the Friedman tests resulted in a $p<0.05$. Post-hoc analyses, for which the α was set at 0.05 ($z = 2.807$), were performed focusing on the following comparisons: 1) step-length and step-height values for baseline vs. first step of the perturbation phase, to test if the perturbation induced a significant change in step length and step height; 2) step-length and step-height values for the first step vs. the last step of the perturbation phase, to test if subjects showed an adaptation to the perturbation force vector; 3) step-length and step-height values for baseline vs. last step of the perturbation phase, to test if subjects fully compensated for the robot-induced changes in step-length and step-height, 4) step-length and step-height values for baseline vs. first step of the aftereffect phase, to test for the presence of a significant aftereffect; 5) step-length and step-height

values for the first step of the perturbation phase vs. the first step of aftereffect phase, to test if the aftereffect mirrored, in magnitude, the robot-induced change in step length and step height; 6) step-length and step-height values for the first step of the aftereffect phase vs. the last step of aftereffect phase, to test if subjects demonstrated changes in step length and step height during this phase; and 7) step-length and step-height values for baseline vs. the last step of aftereffect phase, to test if subjects returned to baseline values of step length and step height at the end of the aftereffect phase. Statistical analysis was used to test for differences between the individual time constants of step length adaptation calculated for each subject in the different phases of the experiments. For this purpose we used Wilcoxon's signed rank test. We compared the following time constants: 1) X perturbation vs. X_{inv} perturbation; 2) X aftereffect vs. X_{inv} aftereffect; 3) X perturbation vs. X aftereffect; 4) X_{inv} perturbation vs. X_{inv} aftereffect; 5) X_{max} perturbation vs. Y_{max} perturbation; 6) X_{max} aftereffect vs Y_{max} aftereffect; 7) X_{max} perturbation vs X_{max} aftereffect; 8) Y_{max} perturbation vs Y_{max} aftereffect. For this analysis α was set at 0.05 and the p-values were adjusted for multiple comparisons using Bonferroni's correction. Statistical analysis was also used to evaluate significant differences in the symmetry indices calculated for step length, step height and mechanical work between the baseline phase and the perturbation phase (last five steps) for all the experiments. This analysis was also based on the Wilcoxon's signed rank test with $\alpha = 0.05$.

Results

Robot-Induced Changes in the Kinematics and Kinetics of Gait

During the experiments, in addition to the step-length and step-height estimates, we generated estimates of the kinematics and kinetics of the hip and knee joints for the right (Figure S06) and the left (Figure S07) lower limbs. Hip and knee torques were derived from the torques measured by the exoskeleton sensors. Figure S06 shows the average - across subjects - hip and knee angles and torques at baseline (black line) and during the first two steps of the perturbation (colored lines) phase of the experiments. Lines in different colors pertain to data collected in different testing

conditions. The plots of Figure S06 on the left-hand side show the data collected in the X, X_{inv} and X_{max} testing conditions. The plots of Figure S07 on the right-hand side show the data collected in the Y, Y_{inv} and Y_{max} testing conditions.

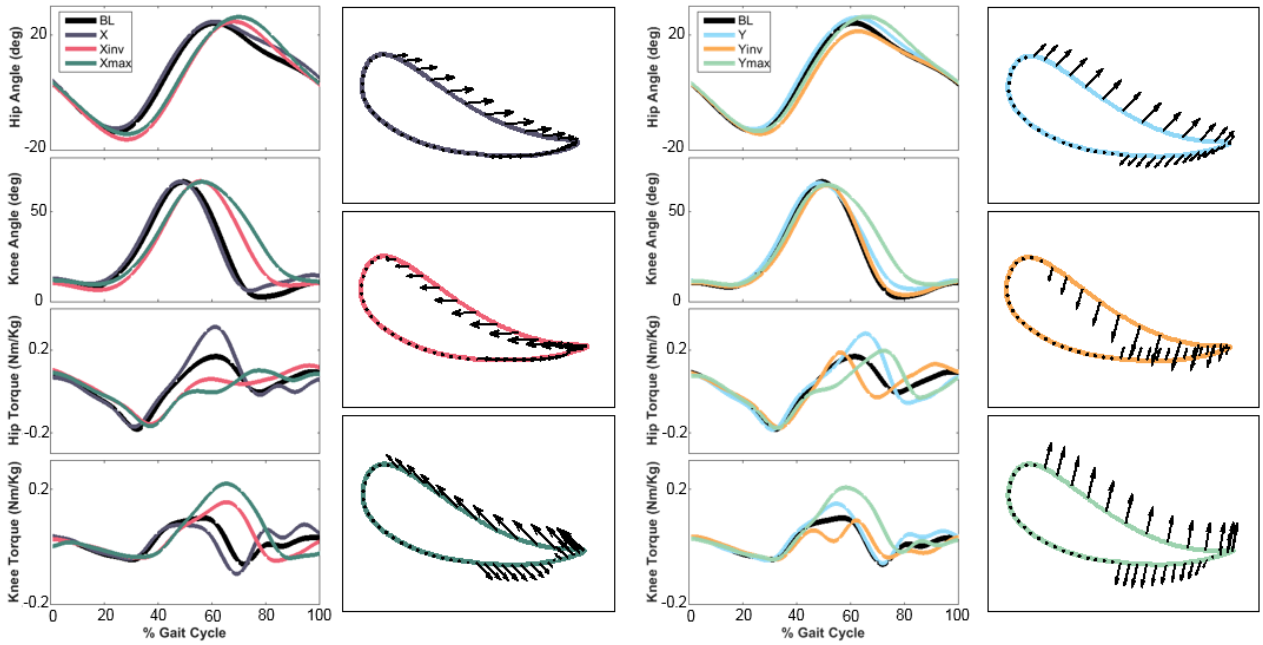

Figure S06: Kinematics and kinetics of motion for the right lower limb during all testing conditions*. The first and third columns show the hip and knee joint angles and torques. The second and forth columns show the reference foot trajectories at baseline in a Cartesian coordinate system attached to the hip joint center of rotation of the exoskeleton system. The black arrows represent the direction of each perturbation.*

The plots showing the hip and knee-joint angles are consistent with the changes in step length and step height observed in each testing condition. For X testing condition, no major changes in hip and knee kinematics are apparent. For the X_{inv} and X_{max} testing conditions, a delayed flexion and extension pattern at both the hip and knee joint compared to baseline is apparent. Moreover, an increase in hip extension torque compared to baseline was observed in the X testing condition, while a decrease in hip extension torque compared to baseline was observed in the X_{inv} and X_{max} testing conditions. In the Y, Y_{inv} and Y_{max} testing conditions we observed very modest changes in the kinematics of gait. More marked changes were observed in the kinetics of gait. In the Y and

Y_{max} testing conditions, we observed an increase in knee and hip flexion torques and a delay in reaching the peak torque value. In the Y_{inv} testing condition, we observed opposite trends.

Figure S07 shows the same plots for the left lower limb. No major changes were observed in the kinematics and kinetics of the left lower limb, other than a temporal shift in the kinematics and kinetics of motion for the X and X_{inv} experiments, consistent with what we observed for the right lower limb.

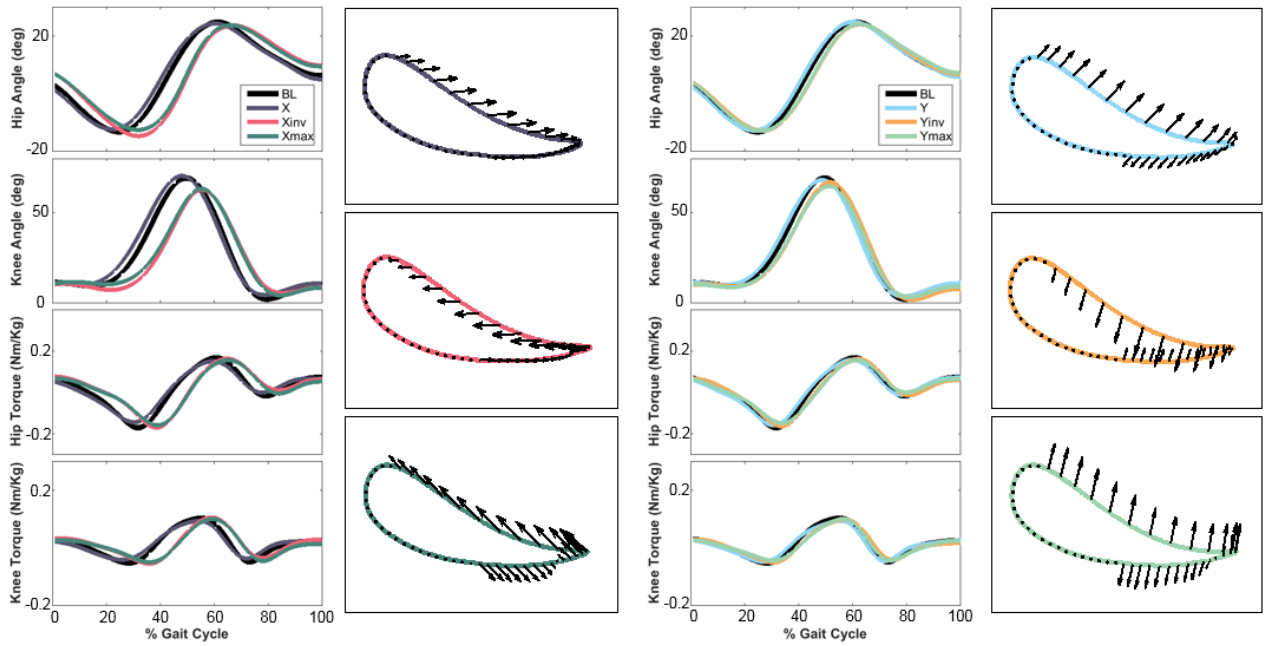

Figure S07: Kinematics and kinetics of motion for the left lower limb during all testing conditions. *The first and third columns show the hip and knee joint angles and torques. The second and forth columns show the reference foot trajectories at baseline in a Cartesian coordinate system attached to the hip joint center of rotation of the exoskeleton system. The black arrows represent the direction of each perturbation.*

Analysis of Step Length and Step Height during the Motor Adaptation Experiments

Statistical analyses confirmed our observation of the presence of motor adaptations and aftereffects in response to a change in step length, and the absence of motor adaptations in response to a change in step height (Figures S08-S13).

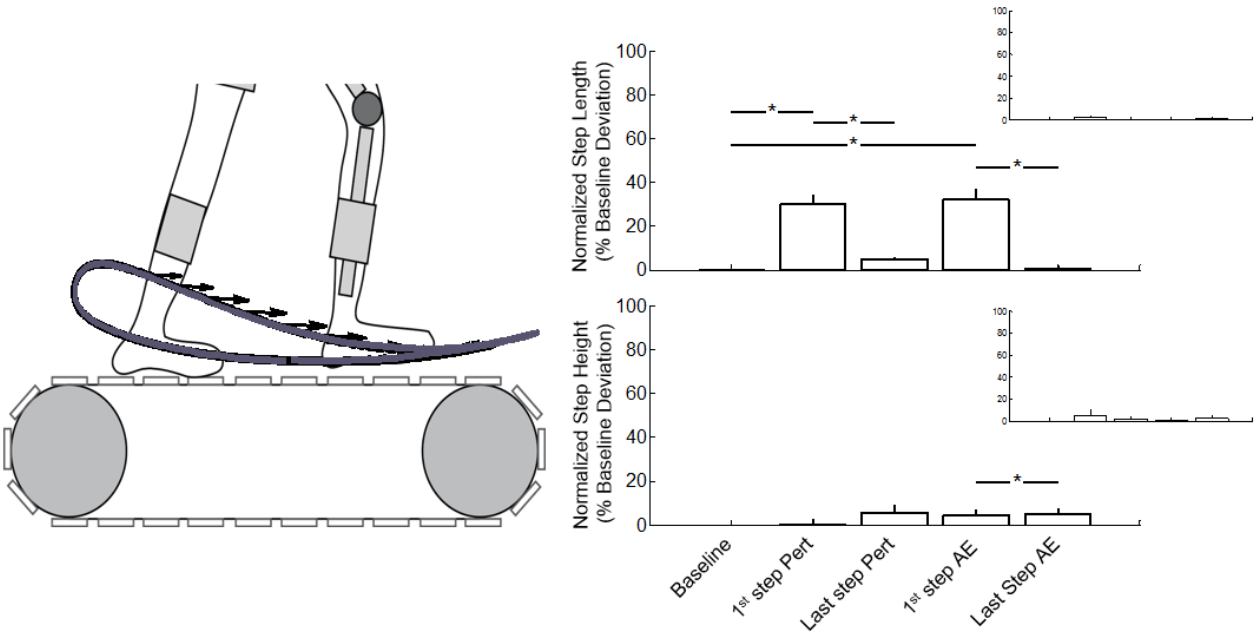

Figure S08: Aggregate results for changes in step length and step height for the X testing condition. *The schematic representation on the left shows the orientation of the perturbation force vector generated by the robot during the perturbation phase. The plot on the top right shows the step length data for the right (larger plot) and the left (inset) lower limbs. The plot on the bottom right shows the step height data for the right (larger plot) and the left (inset) lower limbs. The right lower limb shows motor adaptation in step length but not in step height. The left lower limb does not show changes in step length or step height reflecting motor adaptation. * indicates significant changes among conditions estimated using Friedman tests followed by pair-wise comparisons using the MSD test. Data is shown for: baseline, first step during the perturbation phase (1st step Pert), last step during the perturbation phase (Last step Pert), first step during the aftereffect phase (1st step AE), and last step during the aftereffect phase (Last step AE).*

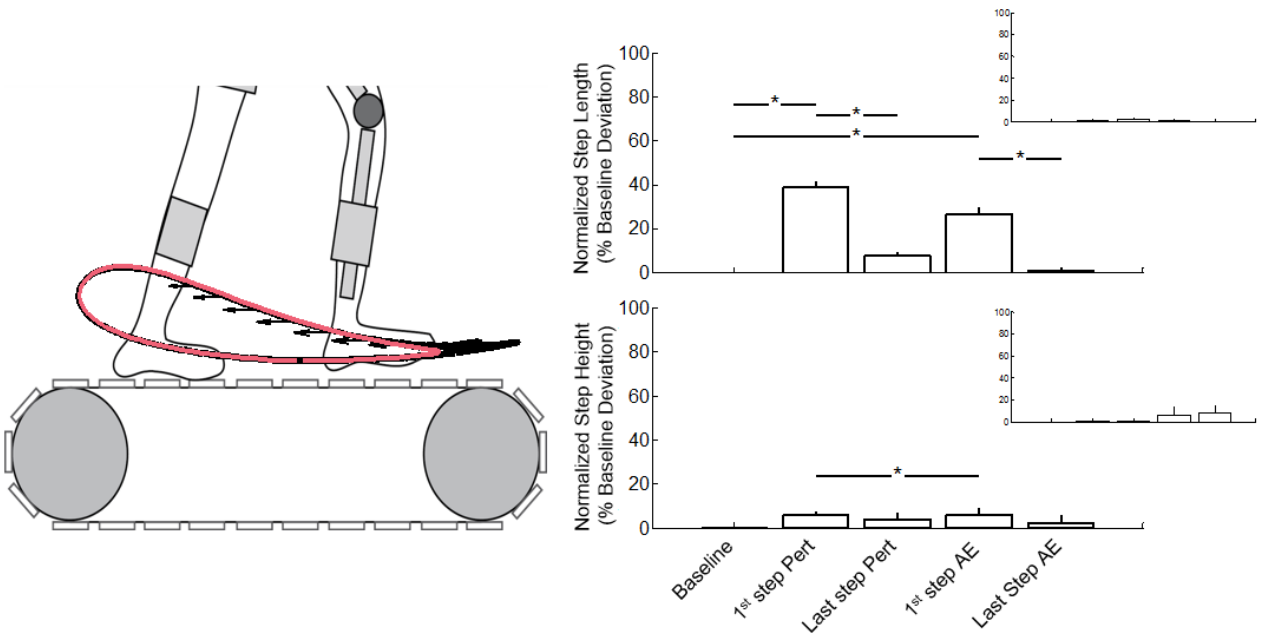

Figure S09: Aggregate results for changes in step length and step height for the X_{inv} testing condition. *The schematic representation on the left shows the orientation of the perturbation force vector generated by the robot during the perturbation phase. The plot on the top right shows the step length data for the right (larger plot) and the left (inset) lower limbs. The plot on the bottom right shows the step height data for the right (larger plot) and the left (inset) lower limbs. The right lower limb shows motor adaptations in step length but not in step height. The left lower limb does not show changes in step length or step height reflecting motor adaptation. * indicates significant changes among conditions estimated using Friedman tests followed by pair-wise comparisons performed using the MSD test. Data is shown for: baseline, first step during the perturbation phase (1^{st} step Pert), last step during the perturbation phase (Last step Pert), first step during the aftereffect phase (1^{st} step AE), and last step during the aftereffect phase (Last step AE).*

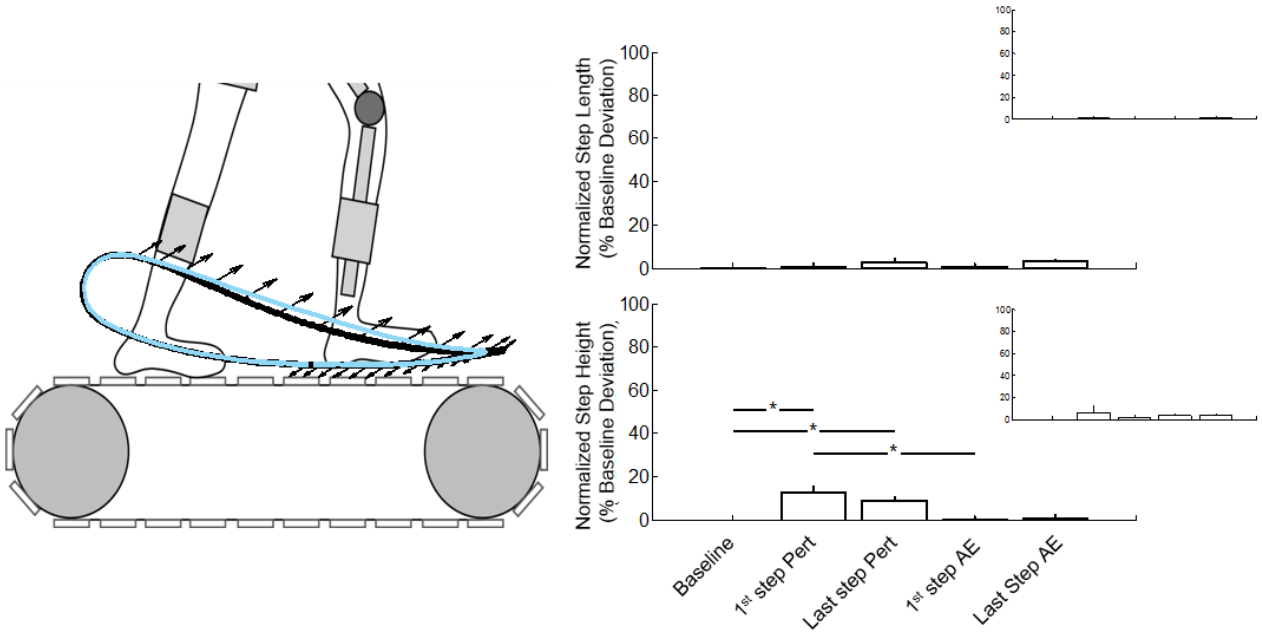

Figure S10: Aggregate results for changes in step length and step height for the Y testing condition*. The schematic representation on the left shows the orientation of the perturbation force vector generated by the robot during the perturbation phase. The plot on the top right shows the step length data for the right (larger plot) and the left (inset) lower limbs. The plot on the bottom right shows the step-height data for the right (larger plot) and the left (inset) lower limbs. The right lower limb does not show motor adaptation. The left lower limb does not show changes in step length or step height reflecting motor adaptation. * indicates significant changes among conditions estimated using Friedman tests followed by pair-wise comparisons performed using the MSD test. Data is shown for: baseline, first step during the perturbation phase (1st step Pert), last step during the perturbation phase (Last step Pert), first step during the aftereffect phase (1st step AE), and last step during the aftereffect phase (Last step AE).*

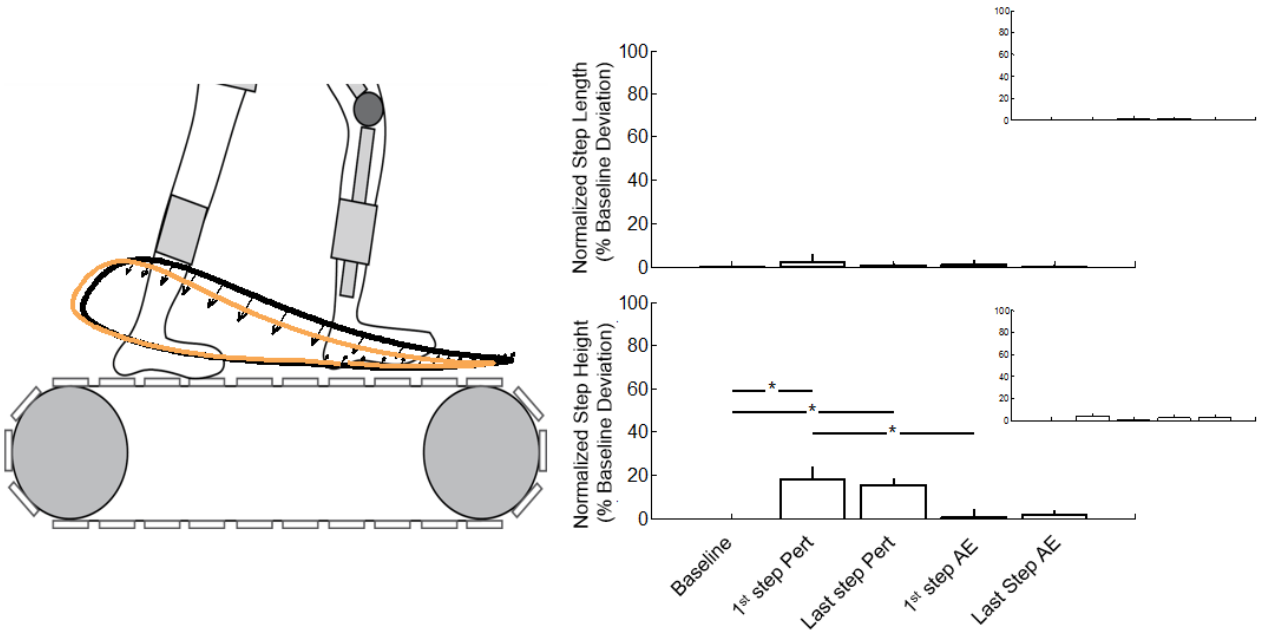

Figure S11: Aggregate results for changes in step length and step height for the Y_{inv} testing condition. *The schematic representation on the left shows the orientation of the perturbation force vector generated by the robot during the perturbation phase. The plot on the top right shows the step length data for the right (larger plot) and the left (inset) lower limbs. The plot on the bottom right shows the step height data for the right (larger plot) and the left (inset) lower limbs. The right lower limb does not show motor adaptation. The left lower limb does not show changes in step length or step height reflecting motor adaptation. * indicates significant changes among conditions estimated using Friedman tests followed by pair-wise comparisons performed using the MSD test. Data is shown for: baseline, first step during the perturbation phase (1st step Pert), last step during the perturbation phase (Last step Pert), first step during the aftereffect phase (1st step AE), and last step during the aftereffect phase (Last step AE).*

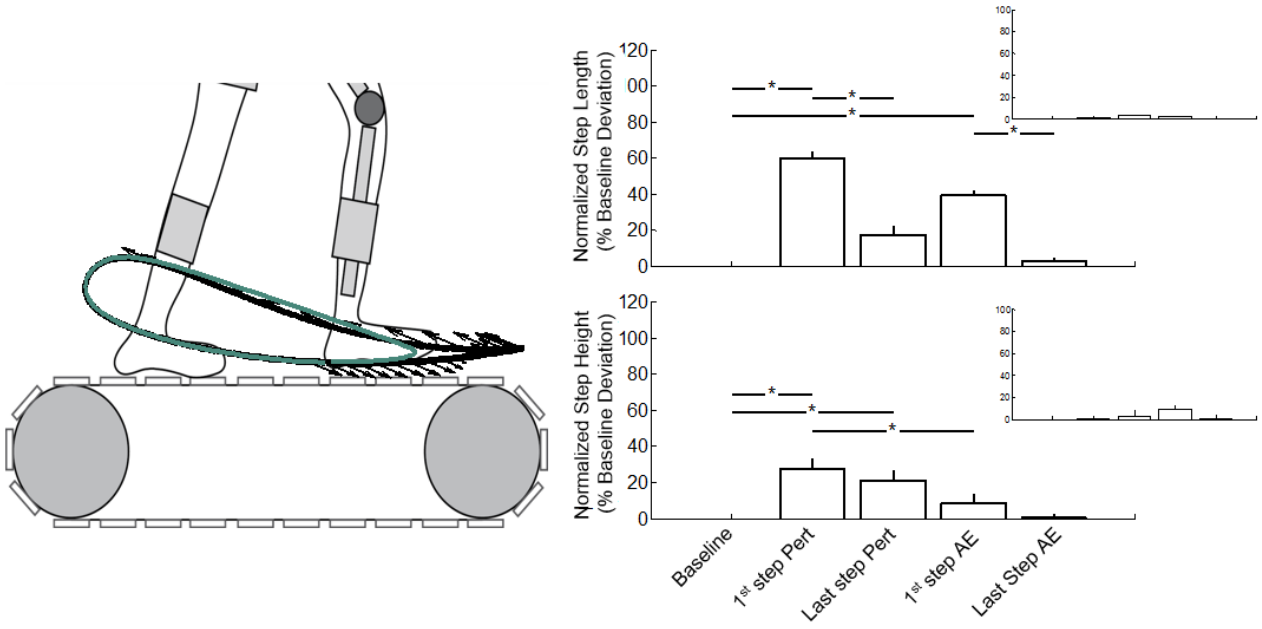

Figure S12: Aggregate results for changes in step length and step height for the X_{max} testing condition. *The schematic representation on the left shows the orientation of the perturbation force vector generated by the robot during the perturbation phase. The plot on the top right shows the step length data for the right (larger plot) and the left (inset) lower limbs. The plot on the bottom right shows the step-height data for the right (larger plot) and the left (inset) lower limbs. The right lower limb shows motor adaptation in step length but not in step height. The left lower limb does not show changes in step length or step height reflecting motor adaptation. * indicates significant changes among conditions estimated using Friedman tests followed by pair-wise comparisons performed using the MSD test. Data is shown for: baseline, first step during the perturbation phase (1^{st} step Pert), last step during the perturbation phase (Last step Pert), first step during the aftereffect phase (1^{st} step AE), and last step during the aftereffect phase (Last step AE).*

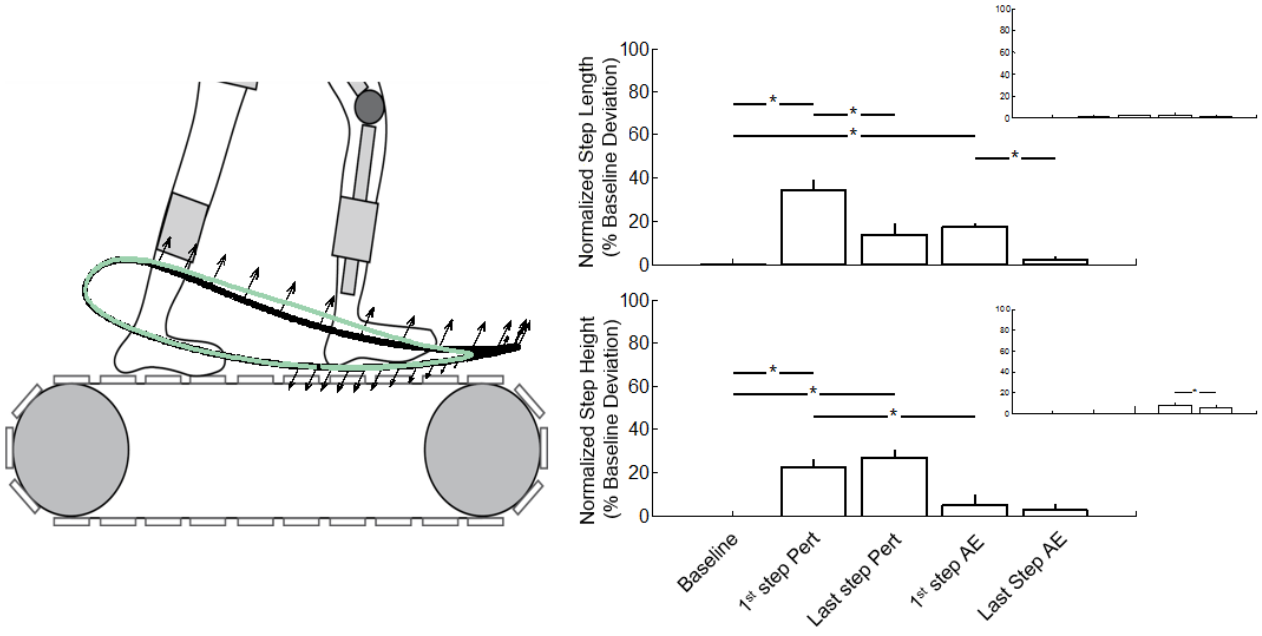

Figure S13: Aggregate results for changes in step length and step height for the Y_{max} testing condition. *The schematic representation on the left shows the orientation of the perturbation force vector generated by the robot during the perturbation phase. The plot on the top right shows the step length data for the right (larger plot) and the left (inset) lower limbs. The plot on the bottom right shows the step height data for the right (larger plot) and the left (inset) lower limbs. The right lower limb shows motor adaptation in step length but not in step height. The left lower limb does not show changes in step length or step height reflecting motor adaptation. * indicates significant changes among conditions estimated using Friedman tests followed by pair-wise comparisons performed using the MSD test. Data is shown for: baseline, first step during the perturbation phase (1^{st} step Pert), last step during the perturbation phase (Last step Pert), first step during the aftereffect phase (1^{st} step AE), and last step during the aftereffect phase (Last step AE).*

Step Length	X	Xinv	Y	Yinv	Xmax	Ymax
BL-1stPert	sig	sig	ns	ns	sig	sig
1stPert-LstPert	sig	sig	ns	ns	sig	sig
BL-LstPert	ns	ns	ns	ns	ns	ns
BL-1stAE	sig	sig	ns	ns	sig	sig
1stPert-1stAE	ns	ns	ns	ns	ns	ns
1stAE-LstAE	sig	sig	ns	ns	sig	sig
BL-LstAE	ns	ns	ns	ns	ns	ns

Step Height	X	Xinv	Y	Yinv	Xmax	Ymax
BL-1stPert	ns	ns	sig	sig	sig	sig
1stPert-LstPert	ns	ns	ns	ns	ns	ns
BL-LstPert	ns	ns	sig	sig	sig	sig
BL-1stAE	ns	ns	ns	ns	ns	ns
1stFF-1stAE	ns	sig	sig	sig	sig	sig
1stAE-LstAE	sig	ns	ns	ns	ns	ns
BL-LstAE	ns	ns	ns	ns	ns	ns

Table S01: Statistical analysis to test for step-length and step-height differences observed during the motor adaptation experiments for all testing conditions. *sig = significant difference (highlighted in green); ns = non-significant difference.*

For the X, X_{inv} ,X_{max} and Y_{max} testing conditions, a significant change in the right step length was observed for the first step of the perturbation phase and the first step of the aftereffect phase of the experiments compared to baseline. Significant changes in the right step height were observed for the Y, Y_{inv}, X_{max} and Y_{max} testing conditions for the first step of the perturbation phase and the first step of the aftereffect phase of the experiments compared to baseline. Motor adaptations were observed for the X, X_{inv}, X_{max} and Y_{max} testing conditions during the perturbation phase of the experiments that resulted in a change in the right step length so that the step length at the end of the perturbation phase was not significantly different from the baseline step-length. In contrast, no adaptations in the right step height were observed for the Y, Y_{inv}, X_{max} and Y_{max} testing conditions. Hence, the right step height at the end of the perturbation phase of the experiments in these testing conditions remained significantly different from the step-height value at baseline. During the aftereffect phase of the experiments, we observed changes consistent with the presence or absence of motor adaptations during the perturbation phase. No significant changes in

step length or step height were observed for the left lower limb. Table S01 summarizes the results of the statistical tests.

	Time constant during adaptation (step length only)	
Condition	Perturbation Phase	Aftereffect Phase
X	3.7±1.6	2.5±0.6
X_{inv}	2.8±0.5	2.2±0.7
X_{max}	5.1±1.4	3.0±1.0
Y_{max}	7.8±2.1	4.3±1.1

Table S02: Time constants of adaptation calculated from the aggregate data (mean ± standard error).

Analysis of the Time-Course of the Motor Adaptations

To quantify the rate of the observed motor adaptations, we used an exponential function to fit the data showing a motor adaptation behavior. The time-course of the motor adaptations was then quantified by using the time constant of the exponential fitting function. Steady state was assumed to be reached within three times the value of the time constant of the exponential fitting function. Time constants were only calculated for the changes in step length observed in the X, X_{inv}, X_{max} and Y_{max} testing conditions. In fact, in these testing conditions, we observed clear patterns of motor adaptation to compensate for changes in step length compared to baseline. As no motor adaptation was observed for changes in step height, time constants were not estimated for step

Time Constant Comparison	p-value
X-Pert vs Xinv-Pert	0.60
X-AE vs Xinv-AE	0.60
X-Pert vs X-AE	0.60
Xinv-Pert vs Xinv-AE	0.39
Xmax-Pert vs Ymax-Pert	0.77
Xmax-AE vs Ymax-AE	0.90
Xmax-Pert vs Xmax-AE	0.23
Ymax-Pert vs Ymax-AE	0.15

Table S03: Comparisons of the values of the time constants derived from individual data associated with motor adaptation for the X, X_{inv}, X_{max} and Y_{max} testing conditions.

height in any testing condition.

Results derived from aggregate data (Table S02) showed that the absolute values of the time constants associated with the motor adaptation spanned from 2.8 to 7.8 steps, indicating that subjects took between 7 to 20 right steps (three times the time constant value) to compensate for the robot-generated perturbation. The absolute values of the time constants associated with the exponential fitting functions for the aftereffect phase of the experiments spanned the range from 2.2 to 4.3 steps, indicating that subjects needed between 7 and 13 right steps to return to the baseline motor behavior. Time constants across testing conditions were found not to be statistically different for the set of comparisons shown in Table S03.

Symmetry Analyses

The analysis of the symmetry indices at baseline and late portion of the perturbation phase of the experiments is summarized in Table S04. For step length, we observed relatively small but statistically significant asymmetric gait patterns for the X_{inv}, X_{max} and Y_{max} testing conditions. It is worth emphasizing that such asymmetries are associated with residual deviations in the step length observed for these experiments at the end of the perturbation phase. For step height, we observed statistically significant asymmetries for all the experiments where this parameter was affected by the robot-generated perturbation. We did not observe asymmetries in step height in the X and the X_{inv} testing conditions, when in fact the perturbations had no effect on step height.

The index calculated to detect asymmetries in the mechanical work generated by the subject showed statistically significant changes for all the testing conditions. The magnitude of the changes in symmetry was lower for the perturbations that did not show motor adaptations. For the X, X_{inv}, X_{max} and Y_{max} experiments, the changes in the kinetics of motion appear to be related to compensating for the perturbation. For the Y and Y_{inv} perturbations, the observed asymmetries appear to denote an adjustment to the robot-generated perturbation that does not have the effect of compensating for the perturbation.

SI - StepLength			
Testing Condition	baseline phase	late perturbation phase	p
X	0.97±0.14	1.03±0.15	0.19
Xinv	1.03±0.06	0.96±0.07	<0.01 (**)
Y	1.03±0.09	1.01±0.09	0.54
Yinv	1.04±0.07	1.02±0.08	0.6
Xmax	1.04±0.08	0.84±0.23	<0.01 (**)
Ymax	1.02±0.08	0.9±0.21	0.04 (*)

SI - StepHeigth			
Testing Condition	baseline phase	late perturbation phase	p
X	0.99±0.19	0.93±0.22	0.15
Xinv	1.18±0.37	1.11±0.20	0.86
Y	1.01±0.20	1.09±0.19	0.02 (*)
Yinv	1.01±0.20	0.89±0.18	0.02 (*)
Xmax	1.11±0.23	1.22±0.25	0.02 (*)
Ymax	0.97±0.22	1.33±0.65	<0.01 (**)

SI - Mechanical Work			
Testing Condition	baseline phase	late perturbation phase	p
X	1.04±0.11	0.38±0.23	<0.01 (**)
Xinv	1.04±0.13	2.72±1.93	<0.01 (**)
Y	1.01±0.18	1.37±0.52	0.03 (*)
Yinv	1.03±0.24	1.41±0.69	0.04 (*)
Xmax	1.02±0.12	5.12±2.23	<0.01 (**)
Ymax	1.03±0.13	2.93±0.77	<0.01 (**)

Table S04: Analysis of the symmetry indices for step length, step height, and the net mechanical work generated by subjects during the baseline and perturbation phases of the motor adaptation experiments. ** indicates p-values < 0.05; ** indicates p-values < 0.01. Significant differences are highlighted in green. These values were estimated using the Wilcoxon's signed rank test.*